

The Percolation Transition in the DNA-Gold Nanoparticle System

Ching-Hwa Kiang and Rona Ramos

Department of Physics & Astronomy, University of California, Los Angeles, CA 90095-1547

Melting and hybridization of DNA-capped gold nanoparticle networks are investigated with optical absorption spectroscopy and transmission electron microscopy. Single-stranded, 12-base DNA-capped gold nanoparticles are linked with complementary, single-stranded, 24-base linker DNA to form particle networks. Compared to free DNA, a sharp melting transition is seen in these networked DNA-nanoparticle systems. The sharpness is explained by percolation transition phenomena.

PACS numbers: 87.15.-v, 87.64.-t, 87.64.Ee

DNA melting and hybridization phenomena are of great importance in both fundamental biological science and biotechnology [1, 2, 3, 4]. Sequence-specific DNA recognition is important in detection, diagnosis of genetic diseases, and identification of infectious agents. Gene chips have been widely used for detecting specific nucleic acid sequences. More recently, DNA-modified gold particles have been used for DNA self-assembly [5, 6]. Organic molecules between gold particles have also been demonstrated to be useful as conducting molecular junctions [7]. DNA-gold nanoparticle systems undergo a change of color upon network formation, which can be used for highly sensitive detection when specific nucleic acid sequences induce network formation [8, 9]. Indeed, such a system has been demonstrated to be useful to detect anthrax and other agents of biowarfare [10].

Our DNA-gold nanoparticle systems were prepared using modified methods based on Ref. [9]. The basic unit is illustrated in Fig. 1. Gold nanoparticles are derivatized with non-complementary, single-stranded, 12-base DNA (4 nm). Upon adding 24-base, complementary linker DNA, particles aggregate to form network structures. These network structures precipitate out of the solution, which produces a visible color change from pink to purple [5].

The DNA-gold nanoparticle system is a model for phase transitions. Melting of short, free DNA is not a phase transition. However, when short DNA are bound to gold particles, the system undergoes a phase transition because the DNA-gold particles form networks of micrometer size, which is approaching a bulk phase. Thus, the binding transition in the network is much sharper

than that of free DNA in solution, due to the cooperative melting process. Many fundamental aspects of phase transitions may be investigated with this biomolecular system.

Here we report studies of DNA-gold nanoparticle melting transitions. We start with a range of different sizes of gold nanoparticles capped with either 3' or 5' modified, single-stranded, 12-base DNA. We then add linker DNA, which causes the nanoparticles to form a network, and we study the melting transition by spectroscopic and microscopic methods. Percolation transition phenomena are observed in the DNA-gold nanoparticle system as it aggregates.

DNA-functionalized gold nanoparticles were prepared by conjugating gold nanoparticles ranging from 10 to 40 nm in diameter (Sigma, ICN Pharmaceutical) with thiol-modified DNA [9, 11]. 3'-alkanethiol DNA 3'S-(CH₂)₃-ATG-CTC-AAC-TCT was prepared by using C3 S-S modifier and 5'-alkanethiol DNA TAG-GAC-TTA-CGC-(CH₂)₆-S5' by C6 S-S on a 1 mol scale and purified by HPLC (Invitrogen). Just prior to conjugation with gold, 100 nmol of the dried DNA was redispersed in 400 μ l of 0.1 M DTT, 0.1 M phosphate buffer (pH 8) solution at room temperature for 30 minutes to cleave the disulfide bond. Salt was removed with a NAP-5 desalting column to avoid bare gold aggregation prior to DNA conjugation.

The deprotected alkanethiol-modified DNA were used to derivatize gold nanoparticles at room temperature for 24 hours to form gold nanoparticle probes. The solutions were then brought to 0.3 M NaCl, 10 mM phosphate buffer (pH 7) and allowed to stand for 48 hours. To remove excess DNA, solutions were centrifuged at 13,200 rpm (16,110 G) for 60 minutes. The supernatant was decanted, and the red precipitate was redispersed in 1 ml nanopure water and centrifuged again. After decanting the supernatant, about 200 μ l of precipitate of each modified gold nanoparticles were collected for spectroscopic investigation.

20 nmol linker DNA 3'GCG-TAA-GTC-CTA-AGA-CTT-GAG-CAT5' (Invitrogen) was dispersed in 1 ml solution of 0.3 M NaCl, 10 mM phosphate buffer (pH 7). Hybridization of linkers with gold nanoparticles was



FIG. 1: Basic building block of gold nanoparticles capped with 12-base DNA with thiol modification at 3' (D1) or 5' (D2) end. L is linker DNA composed of 24-base DNA complementary to the capping DNA D1 and D2. Capping DNA is bound to gold nanoparticles through covalent bonds, and the linker DNA L binds the capping DNA through hydrogen bonds.

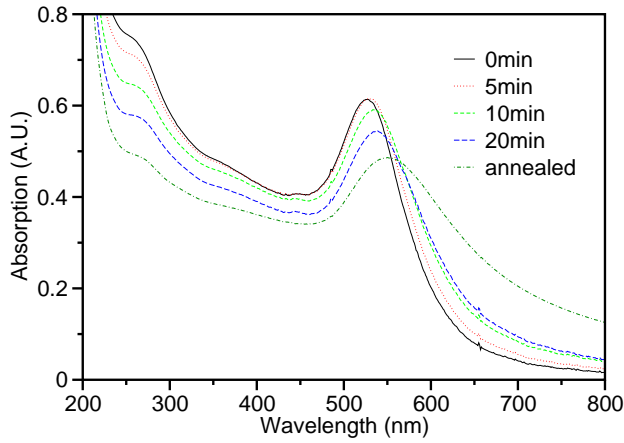


FIG. 2: Optical absorption spectra of DNA-modified gold nanoparticles. The time starts when linker L is added to the solution containing mixtures of gold nanoparticles modified with D1 and D2. Owing to the particle network formation, the 520 nm gold surface plasmon peak slowly shifts to longer wavelength, followed by peak broadening and further shifting.

done by mixing 200 μ l each modified gold nanoparticles (0.8 OD) with 8 μ l linker solution (10 pmol/ μ l). The solution was annealed at 70 $^{\circ}$ C for 10 minutes and cooled to room temperature during a 2 hour period and was allowed to aggregate for several days.

Absorption spectra of DNA-modified gold nanoparticles were taken on a Hewlett-Packard diode array spectrophotometer (HP 8453). The kinetics of formation of network nanoparticle structures at room temperature is illustrated in Fig. 2. Upon adding linker DNA, gold nanoparticles aggregate to form networks, as demonstrated in the gold surface plasmon peak (520 nm) shift of the DNA-modified gold nanoparticles [12, 13, 14]. The aggregation started with the wavelength shift of the plasmon band, followed by broadening and more shifting of the peak as hybridization continues. From molecular simulations it is known that change in network size results mainly in peak broadening, whereas change in gold volume fraction results mainly in peak shifting [13]. Our results indicate that the initial aggregation has characteristics consistent with increasing volume fraction, followed by increasing network size.

To study the equilibrium behavior of DNA-gold nanoparticle system, we monitor the UV-visible spectra absorption intensity at 260 nm and 520 nm while melting the DNA-gold nanoparticle network. DNA bases have strong absorption at the UV region, and the peak near 260 nm is a result of combination of these electronic transition dipoles [15]. The DNA double helix has smaller extinction coefficient than single-stranded DNA due to hypochromism and, therefore, the absorption intensity at 260 nm increases as a result of DNA melting. The sample was heated by a peltier temperature controller (JASCO J-715) at a rate of 0.5 $^{\circ}$ C/min, from 25 to 75 $^{\circ}$ C. The

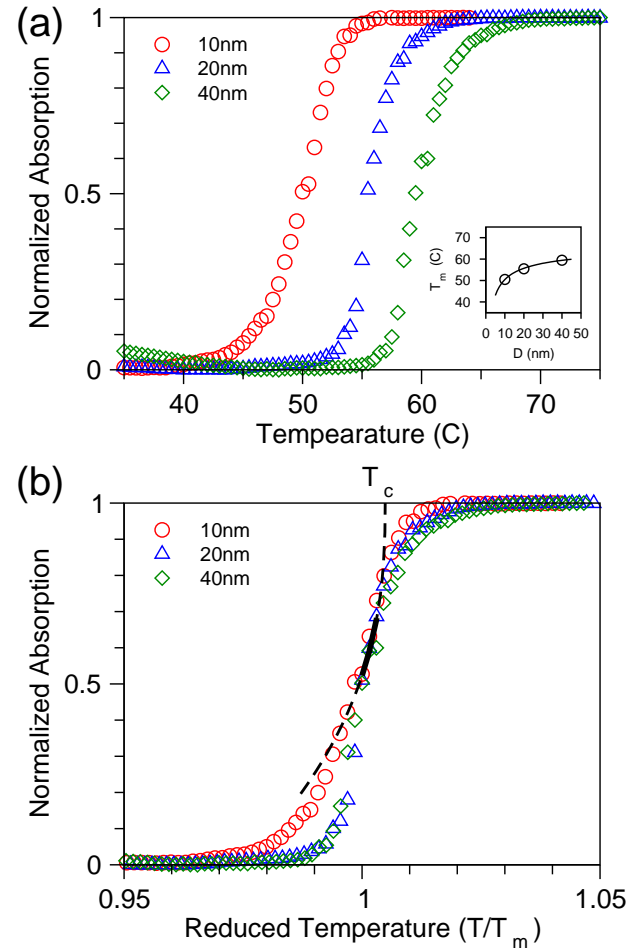


FIG. 3: Normalized melting curves of linked gold nanoparticle networks monitored at 260 nm. (a) Melting curves of different size particles as a function of temperature. Inset shows the change in melting temperature, T_m , with particle diameter D . Data are fitted with a power law. (b) Melting of particles as a function of reduced temperature. Solid line shows the region where data were used for curve fitting, dashed line is calculated from the equation of best fit (see text). The scaling shows the universality of the melting transition above the transition temperatures.

260 nm and 520 nm melting curves are very similar, indicating that DNA and nanoparticle melting are closely related. Figure 3a displays the melting curves of 10 nm, 20 nm, and 40 nm gold particles with linker DNA. The melting transition width (FWHM) is about 5 $^{\circ}$ C, compared to 12 $^{\circ}$ C for melting of free DNA [8]. As illustrated in the figure, the transition width as well as the melting temperature T_m of DNA have been dramatically modified by the binding to gold particles.

The melting temperature T_m , defined as the temperature at the midpoint of the absorbance transition [16], is found to be a function of particle diameter, D , and the data are fitted to $T_m (^{\circ}\text{C}) = 68 - 57/D$. The surface coverage of thiol-capped DNA bound to gold nanoparti-

cles has been determined via the fluorescence method to be approximately 160 DNA (12-mer) bound for a 16 nm diameter particle [17]. Assuming the number of DNA bound to gold particles scales with the particle surface area, D^2 , there are 50, 190, and 750 DNA on 10 nm, 20 nm, and 40 nm particles, respectively. An increasing number of connections between particles as the gold particle size increases is expected. Since the hydrogen bonding energy per DNA pair remain the same, an increased number of connections effectively increases the enthalpy, H , between particles and, therefore, raises the melting temperature T_m .

For short DNA (12{14 base pairs), melting and hybridization can be described by a two-state model as an equilibrium between single- and double-stranded DNA [16], $S + S \rightleftharpoons D$. The melting curve is a slowly varying function of temperature and can be described by the van't Hoff relationship [15]. While short, free DNA does not exhibit a phase transition, DNA bound to nanoparticles aggregate to form networks that have a definite phase transition, and the melting curves cannot be described with the van't Hoff relationship.

Figure 3b illustrates two different transitions at high T and low T . The absorption of DNA-modified, 10 nm, 20 nm, and 40 nm gold nanoparticles are plotted versus reduced temperatures ($T_R = T/T_m$). Above temperature T_m (low connectivity), the curves appear insensitive to details, indicative of universal scaling at the percolation transition [18]. The curves can be fitted with an equation that describes percolation phenomena,

$$A(T_R) = 1 - a(T_c - T_R)$$

where $A(T_R)$ is the absorption as a function of reduced temperature T_R , and a is the critical exponent for percolation. In three-dimensions, $a = 0.403$ [19]. The parameters a and T_c are adjustable. Using the data for all three particle sizes for $1 < T_R < 1.003$, we obtained $a = 4.079$ and $T_c = 1.005$, as shown in Fig. 3b. The deviation from the fit above T_c is presumably due to finite size effects [20].

The fitted curve demonstrates that the transition from single- to double stranded DNA in the DNA-gold nanoparticle system can be explained by percolation. Percolation phenomena occur when the gold particles make enough connections to other gold particles, and networks of nearly infinite clusters form [19, 21]. Gold particles make more connections at lower T because there are more hydrogen bonds between the double helix at lower T , therefore, percolation begins to occur at lower T . The equilibrium constant, K_{eq} for reaction $S + S \rightleftharpoons D$, is analogous to the probability of a bond in the "bond percolation" model.

Transmission electron microscopy (TEM) of DNA-modified, 10 nm gold particle systems at various stages of growth are shown in Fig. 4. TEM samples were prepared by letting 5 μ l of solution containing particles dry on a

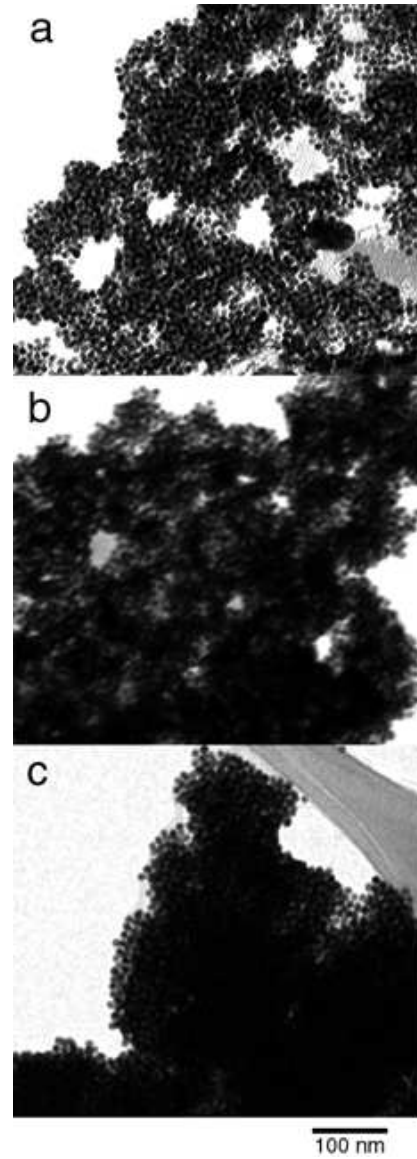


FIG. 4: Transmission electron microscopy of networks of 10 nm gold nanoparticles capped with thiol-modified DNA. (a) Initial growth stage of nanoparticle network. The structure is porous and amorphous. The sample was isolated 10 minutes after the linker DNA was added. (b) The network continues to grow past the percolation threshold. The sample was isolated 20 minutes after linker DNA was added. (c) Dense network formed after annealing. The aggregates correspond to points on the melting curve (a) slightly above the percolation transition temperature T_c , (b) near and above the melting temperature T_m , and (c) far below the melting temperature in Fig. 3b. The corresponding UV-visible spectra are shown in Fig. 2

lacey carbon grid. Images were taken on a LEO 912 transmission electron microscope operated at 120KV. The TEM was equipped with an Omega image filter, and the images were captured with a Gatan slow-scan camera at 20,000 to 80,000 magnifications. Only the material

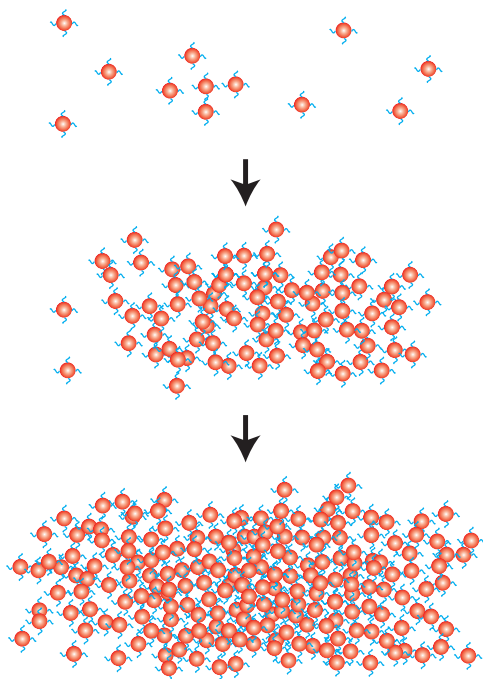


FIG. 5: Growth mechanism of the DNA-gold nanoparticle network. When linker DNA is added, hybridization occurs, connecting the gold nanoparticle into porous networks. As the cluster grows, the volume fraction and the size of the cluster continue to increase. The transition between dispersed nanoparticles and micrometer sized cluster appears to be a cooperative phenomenon [22], much like a phase transition.

over the holes in the grid, not on the carbon support, were used for interpreting their structures, because particles form two dimensional crystalline aggregates on the carbon support. Even in absence of linker DNA [14].

Figure 4a is a TEM image of DNA-modified, 10 nm gold nanoparticles at the start of aggregation. This stage is equivalent to the onset of percolation (55°C) in Fig. 3a. Figure 4b is near the percolation threshold T_c (52°C), showing a porous, amorphous network structure. Figure 4c is an annealed network, representative of the low temperature (room temperature) structure, which formed dense networks.

The growth mechanism of the DNA-gold nanoparticle network is illustrated in Figure 5. Particles initially are dissolved in the solution. With the addition of complementary linker DNA, hybridization occurs, and the particles form a network-like structure. The volume fraction of the porous structure continues to increase past the percolation threshold, and eventually the clusters become a dense amorphous structure.

In conclusion, the network formation in DNA-gold particle systems exhibits a phase transition, which does not occur for short DNA. Our results provide detailed and precise measurements of hybridization/melting of the DNA-gold nanoparticle system. DNA attached to gold is a controlled system in which to do experiments on phase

transitions and serves as a good probe for many biological systems that involve DNA. This is a new system, about which relatively little is known. Many parameters, such as the length of DNA, particle size, degree of disorder, solution pH value, and salt concentration, may be varied to better understand the system.

To whom correspondence should be addressed, Email: chkiang@physics.ucla.edu.

-
- [1] R. M. Wortell and A. S. Benight, *Phys. Rep.* **126**, 67 (1985).
 - [2] D. Cule and T. Hwa, *Phys. Rev. Lett.* **79**, 2375 (1997).
 - [3] C. A. Gelfand, G. E. Plum, S. M. Jelewicz, D. P. Remeta, and K. J. Breslau, *Proc. Natl. Acad. Sci. USA* **96**, 6113 (1999).
 - [4] N. L. G. Oddard, G. Bonnet, O. Krichinsky, and A. Libchaber, *Phys. Rev. Lett.* **85**, 2400 (2000).
 - [5] C. A. Mirkin, R. L. Letsinger, R. C. Mucic, and J. J. Storho, *Nature* **382**, 607 (1996).
 - [6] A. P. Alivisatos, K. P. Johnsson, X. Peng, T. E. Wilson, C. J. Loweth, M. P. Bruchez Jr., and P. G. Schultz, *Nature* **382**, 609 (1996).
 - [7] M. A. Reed, C. Zhou, C. J. Muller, T. P. Burgin, and J. M. Tour, *Science* **278**, 252 (1997).
 - [8] R. Elghanian, J. J. Storho, R. C. Mucic, R. L. Letsinger, and C. A. Mirkin, *Science* **277**, 1078 (1997).
 - [9] J. J. Storho, R. Elghanian, R. C. Mucic, C. A. Mirkin, and R. L. Letsinger, *J. Am. Chem. Soc.* **120**, 1959 (1998).
 - [10] C. A. Mirkin, *Inorg. Chem.* **39**, 2258 (2000).
 - [11] L. A. Chrissy, G. U. Lee, and C. E. O'Ferrall, *Nucleic Acids Res.* **24**, 3031 (1996).
 - [12] A. A. Lazarides and G. C. Schatz, *J. Phys. Chem. B* **104**, 460 (2000).
 - [13] J. J. Storho, A. A. Lazarides, R. C. Mucic, C. A. Mirkin, R. L. Letsinger, and G. C. Schatz, *J. Am. Chem. Soc.* **122**, 4640 (2000).
 - [14] S. Link and M. A. El-Sayed, *J. Phys. Chem.* **103**, 8410 (1999).
 - [15] C. R. Cantor and P. R. Schimmel, eds., *Biophysical Chemistry, Part II: Techniques for the study of biological structure and function* (W. H. Freeman and Company, New York, 1980).
 - [16] V. A. Bloomfield, D. M. Crothers, and I. Tinoco, Jr., *Nucleic Acids* (University Science Books, California, 2000).
 - [17] L. M. Demers, C. A. Mirkin, R. C. Mucic, R. A. Reynolds, III, R. L. Letsinger, R. Elghanian, and G. V. Sivanadham, *Anal. Chem.* **72**, 5535 (2000).
 - [18] J. Rudnick, P. N. Akmal, and G. G. Aspari, *Phys. Rev. E* **58**, 5596 (1998).
 - [19] R. J. Creswick, H. A. Farach, and C. P. Poole, Jr., *Introduction to Renormalization Group Methods in Physics* (John Wiley & Sons, New York, 1992), pp. 69-107.
 - [20] M. W. Deem and J. M. Newsum, *J. Phys. Chem.* **99**, 14903 (1995).
 - [21] H. E. Stanley, J. S. Andrade Jr., S. Havlin, H. A. Makse, and B. Suki, *Physica A* **266**, 5 (1999).
 - [22] J. Rudnick and R. Bruinsma, *Biophys. J.* **76**, 1725 (1999).